Magneto-optical investigation of flux penetration in a superconducting ring

Myriam Pannetier,* F. C. Klaassen, R. J. Wijngaarden,† M. Welling, K. Heeck, J. M. Huijbregtse, B. Dam, and R. Griessen

Faculty of Sciences, Division of Physics and Astronomy, Vrije Universiteit De Boelelaan 1081, 1081 HV Amsterdam, The Netherlands
(Received 12 April 2001; published 18 September 2001)

Using advanced magneto-optics, the field and current *distributions* in superconducting thin film $YBa_2Cu_3O_7$ rings in an externally applied magnetic field are studied experimentally. The observations are in close agreement with numerical calculations. During the initial flux penetration and field reversal a highly nonuniform current distribution is observed. In particular, concentric counterrotating current loops occur during field reversal. We explore implications of these results for the determination of critical currents and penetration fields from bulk magnetization measurements.

I. INTRODUCTION

In many studies on superconductors, ring-shaped samples are used, to measure, e.g., the flux relaxation rate,[1] the magnetic flux noise,[2] the levitation forces,[3] or the photoresponse in the flux creep regime.[4] In order to determine the critical currents[5–8] in superconductors, thin-film rings were used because of the well-defined shape and constant sample width perpendicular to the current flow direction. The interpretation of all these experiments presupposes knowledge of the current distribution. Most authors assume that this current distribution is uniform.

Theoretically, the behavior of rings and disks seems well established.[9,10] Experimentally, however, these predictions have not been verified in detail, which is surprising in view of the amount of data based on measurements on such samples. In addition, ringlike shapes also occur in practical applications, e.g., in superconducting quantum interferences device (SQUID) loops. For these reasons an experimental investigation of the exact current distribution in ring-shaped samples is strongly needed. Our findings, using the recently improved magneto-optical technique, are presented in this paper.

The magneto-optical technique[11] enables a direct measurement of the magnetic field above the superconductor, from which the current distribution can be derived[12–14] for a two-dimensional geometry. A recent improvement[15] of the technique enables an accurate and linear measurement of the local magnetic field, including an unambiguous determination of its sign. Results are presented for two superconducting rings with different widths. It is found that during part of the hysteresis loop, the field and current distributions exhibit a peculiar behavior, with alternating positive and negative domains within the width of the ring.

This paper is organized as follow: the details of the samples and the experimental technique are presented in Sec. II. The numerical calculations used for direct comparison with the experiment are described in Sec. III. Experimental results are given in Sec. IV, with emphasis on two aspects: the first penetration after zero-field cooldown and the reversal of the sweep direction of the applied magnetic field.

II. EXPERIMENT

A. Samples

Results are presented here for two rings patterned from $YBa_2Cu_3O_{7-\delta}$ thin films, deposited by means of pulsed laser deposition on (100) $SrTiO_3$ substrates. Similar results are obtained on other rings. The thickness of the rings is 100 nm and the critical temperature is 90 K, with $\Delta T < 0.5$ K. The samples are characterized by Rutherford backscattering, atomic force microscopy, and x-ray diffraction (XRD).[16] The excellent crystallinity of these films enables even the observation of Laue finite-size oscillations around the (001) reflection of the XRD spectrum.[17]

The films are patterned into rings using conventional photolithography and chemical etching in H_3PO_4. The rings have an outer diameter of 3 mm, a width of 500 μm for ring 1, and 125 μm for ring 2. The samples are checked for irregularities, scratches, and weak spots by optical transmission and reflection microscopy and exhibit excellent quality. Subsequently magneto-optics showed no inhomogeneous flux penetration along the circumference.

The rings are investigated by means of torque magnetometry and magneto-optical imaging in order to make a direct comparison *on the same samples* between the bulk magnetic moment as determined from torque and the current and field distribution as determined from magneto-optics.

B. Torque magnetometry

The penetration field and the superconducting current density are measured by means of capacitive torque magnetometry.[5,18] The sample is placed in a magnetic field $\mu_0\vec{H}$ with its normal at a small angle θ with the applied field. When the applied field is increased at a constant sweep rate $\mu_0 dH/dt$, superconducting currents are induced in the sample. The corresponding magnetic moment $\vec{M}_{irr}$ leads to a torque $\vec{\tau}$ given by

$$\vec{\tau} = \mu_0(\vec{M} \times \vec{H}). \tag{1}$$

The irreversible torque $\vec{\tau}_{irr}$ at a certain magnetic field is given by

$$\tau_{irr} = (\tau_+ - \tau_-)/2, \tag{2}$$

τ_+ and τ_- being the ascending and descending branches of a magnetic hysteresis loop. The irreversible magnetic moment is then given by

$$M_{irr} = \tau_{irr}/(\mu_0 H \sin \theta), \tag{3}$$

since $\vec{M}$ is perpendicular to the film plane.

In the case of a uniform current density, the current density j_s is directly related to the magnetic moment of a ring of inner radius a_1, outer radius a_2, and thickness d by

$$M_{irr} = (\pi/3)d(a_2^3 - a_1^3)j_s. \tag{4}$$

The torque magnetometer is placed into the variable temperature insert of a 7-T Oxford Instruments Magnet system. The cryostat enables measurements from 1.5 K up to 300 K. The magnetic field is applied at an angle $\theta = 10°$. Experiments are performed after zero-field cooling (ZFC) by looping the field from zero to $+200$ mT, then to -200 mT, and again to $+200$ mT, with a constant sweep rate of 1 mT/s.

C. Magneto-optical imaging

In the magneto-optical (MO) experiments, the local magnetic field immediately above the sample is detected using Bi-doped yttrium iron garnet films[19] with in-plane anisotropy, which exhibit a large Faraday effect (typically 0.06 deg/mT) and can be used for a broad range of temperatures, from 1.5 K up to 300 K. The magnetic resolution is better than 0.1 mT and the spatial resolution is better than 0.5 μm.

The indicator is placed on top of the sample and the assembly is mounted in our specially built cryogenic polarization microscope,[11] which is in a magnet system similar to the one described above. The applied magnetic field is parallel to the c axis of the sample and perpendicular to the indicator. We use two types of measurements: (i) *conventional magneto-optics* between two crossed polarizers; the spatial variation of the perpendicular component of the local induction B_z at the sample is visualized as an intensity pattern; from the intensity images, the local field H_z is determined using the calibration $I = bf(H_z^2)$, where I is the intensity and b is a proportionality constant.[20] (ii) using our new *magneto-optical image lock-in amplifier* (*MO-ILIA*) setup,[15] the local magnetic field is measured directly as an output of the MO-ILIA. The second technique is a considerable improvement due to the intrinsic linearity in field, the direct measurement of the sign of the field, and the improved sensitivity at small magnetic fields.

Experiments presented here are performed at $T = 4.2$ K, after ZFC by looping the field from zero to $+50$ mT, then to -50 mT , and again to $+50$ mT, with a constant sweep rate of 1 mT/s. No qualitative differences were observed for different sweep rates. The pictures are taken effectively every second with a charge-coupled device (CCD) camera [hence the difference in field between consecutive pictures is $\Delta(\mu_0 H) = 1$ mT].

III. NUMERICAL SIMULATION

In order to obtain a complete description and a full understanding of the phenomena occurring in the ring, we investigate the distribution of the current density while performing a hysteresis loop. Since there exists significant relaxation in high-temperature superconductors, we simulate the behavior of superconducting rings with the model of Brandt,[10] which takes relaxation into account. With the help of this simulation, in which we include our experimental conditions, we can calculate numerically the field profiles and current distributions in the sample. A numerical calculation is required due to the geometry: the elliptic integrals of the problem make it analytically untractable (see Brandt[10]).

Our calculation is based on that of Brandt, which expresses the time derivative of the position-dependent current in the ring as a function of the current and sweep rate of the externally applied field. To derive this recursive difference equation, we note that the vector potential $\vec{A}$ depends, due to the radial symmetry, in the plane of the ring only on the radius r. In addition, only the A_ϕ component is nonzero.

The vector potential for a single loop of current of radius a is given by[21]

$$A_\varphi(r, \theta) = \frac{\mu_0}{4\pi} Ia \int_0^{2\pi} \frac{\cos \varphi' d\varphi'}{(a^2 + r^2 - 2ar \sin \theta \cos \varphi')^{1/2}}. \tag{5}$$

Hence, for a very thin ring of thickness d, inner diameter a_1, and outer diameter a_2,

$$A_\varphi(r, \theta) = \frac{\mu_0}{4\pi} \int_{a_1}^{a_2} I(a')a'$$

$$\times \int_0^{2\pi} \frac{\cos \varphi' d\varphi'}{(a'^2 + r^2 - 2a'r \sin \theta \cos \varphi')^{1/2}} da'. \tag{6}$$

Note that we use here the current $I(a')da'$ flowing at radius a' which is related to the current density j by $I = j*d$.

Using $\theta = \pi/2$ for the plane of the ring and by discretizing the space on the width of ring, we obtain

$$A_\phi(r) = \frac{\mu_0}{4\pi} \sum_{p=a_1}^{a_2} I(p)p \int_0^{2\pi} \frac{\cos \varphi' d\varphi'}{(p^2 + r^2 - 2pr \cos \varphi')^{1/2}}$$

$$=: \frac{\mu_0}{4\pi} \sum_{p=a_1}^{a_2} I(p)Q(p,r), \tag{7}$$

where $I(p)$ is now the current flowing between $p - \frac{1}{2}\Delta a$ and $p + \frac{1}{2}\Delta a$, Δa being the grid spacing and the second equal sign defines a kernel matrix Q.

In matrix notation, Eq. (7) may be abbreviated as

$$\vec{A}_\phi = \frac{\mu_0}{4\pi} \vec{\vec{Q}} \cdot \vec{I}. \tag{8}$$

Here and below the arrow on A_ϕ and I is used to denote the position-dependent quantities written as a mathematical vector in discretized space.

The total vector potential is due to the current in the ring and the external field:

$$A_{\phi,tot} = A_{\phi,ring} + A_{\phi,ext}. \tag{9}$$

For a uniform external field along the $\hat{z}$ axis, $A_{\phi,ext} = \mu_0(r/2)H_z$. Inserting this and Eq. (8) into Eq. (9) gives:

$$\frac{\mu_0}{4\pi}(\vec{Q} \cdot \vec{I}) = A_{\phi,tot} - \mu_0 \frac{r}{2} H_z. \tag{10}$$

To proceed we need the relation between current density j and electrical field E in the superconductor. For simplicity[10] we use a power-law relation for the resistivity:

$$E = \rho j = \rho_0 \left| \frac{j}{j_0} \right|^{\sigma} j = R_0 |I|^{\sigma} I. \tag{11}$$

For large σ this captures the essential superconductor physics, where the electrical field rises sharply when the current density exceeds the value j_0 (close to the critical current density j_c), while it is very convenient in the calculation.

By taking the time derivative of Eq. (10) and using $\dot{A}_{\phi,tot} = \dot{A}_{tot} = -E = -\rho j,$[21] with ρ from Eq. (11) one obtains the following equation:

$$\frac{\partial \vec{I}}{\partial t} = \left(\frac{4\pi}{\mu_0} \right) \vec{Q}^{-1} \cdot \left(-R_0 |\vec{I}|^{\sigma} \vec{I} - \mu_0 \frac{r}{2} \dot{H}_z \right), \tag{12}$$

Equation (12) can be easily iterated numerically. The initial condition at $t=0$ is set to zero current all over the width of the ring. The applied field may be chosen to increase linearly with time to compare with the experimental situation where the sweep rate is constant. Also a complete hysteresis loop can be easily calculated. From the current $I(r)$ in the ring, the magnetic field in all space around the ring is also calculated, taking into account the external field (obtained from integration of $\dot{H}_z$).

IV. RESULTS AND ANALYSIS

We now compare the experimental magnetic moment M_{irr} obtained from torque measurements with magneto-optical data on the local field H_{tot} perpendicular to the plane of the ring. In addition, both types of experimental results are compared with our numerical simulations.

A. First penetration and penetration fields

In the magneto-optical experiment, as soon as a positive external field is applied to a ZFC sample, there is not only an intense bright outline at the outer edge of the ring (Fig.1), due to an enhancement of the external field by the shielding currents. Surprisingly there is also an intense dark outline at the inner edge of the ring, corresponding to a local field opposite to the applied field and initially increasing in strength with B_{ext}. This is rather unexpected: a negative field is generated in the inside of the ring before full penetration, i.e., before vortices reach the inner edge (after having crossed the whole width of the ring). This effect is due to the
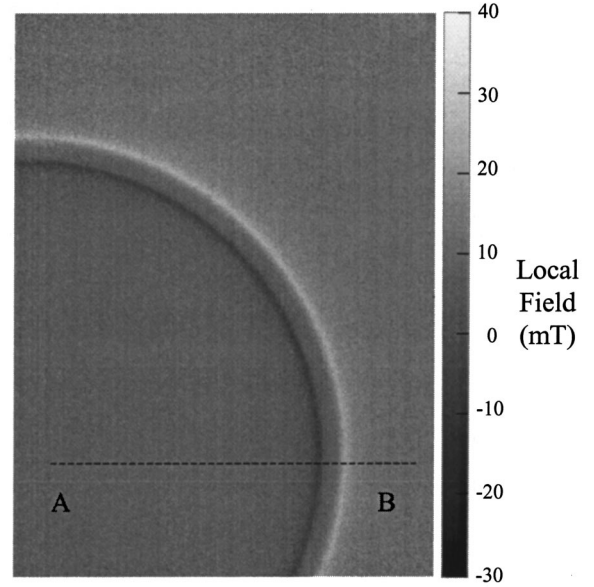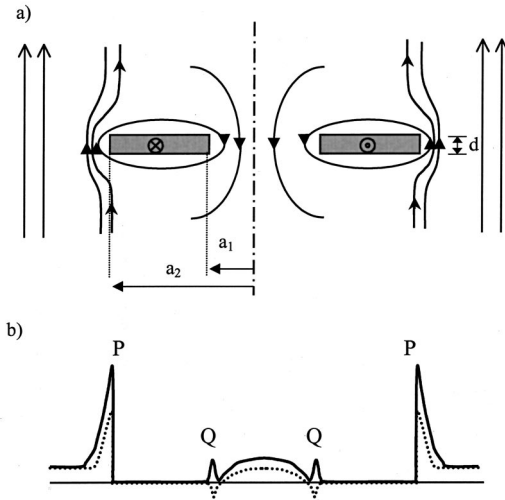

FIG. 1. Local field map obtained from MO-ILIA (see text) magneto-optical imaging of ring 2 (125 μm width), with an applied field of 8 mT, at $T=4.2$ K. The scale bar gives the local field values in mT. We observe a positive bright outline at the outer edge of the ring, while a negative dark outline is visible at the inner edge of the ring. The profiles shown in Figs. 3(a) and 6(a) are measured along the dashed line AB.

fact that the shielding currents cannot drop off slowly towards zero in the center of the ring, but must be zero inside its inner perimeter. One way of describing this[22] is that our ring is equivalent to the superposition of a superconducting disk with the same outer diameter as the ring and ordinary shielding currents and a disk with same outer diameter as the inner diameter of the ring and counterflowing shielding currents. The latter currents produce at the edge of the inner virtual disk a peaked field, which is negative because the currents are counterflowing. Another way to look at this is as follows. If we consider the ring in the virgin state, there is no flux anywhere (inside and outside). Then when a magnetic field is applied, perpendicular to the film, a supercurrent will flow in the ring, in order to keep it in the Meissner state. On the outer edge of the ring, the field generated by the shielding currents adds to the applied field [see Fig. 2(a)], as in the flat strip case (see, for example, Ref. 23). This results in a sharp peak P at the outer edge [Fig. 2(b)], increasing with the applied field. But because of the geometry of the ring, the flux lines of the self-field close by threading through the hole [see Fig. 2(a)], thereby generating a negative field at the edge of the hole [peak Q in Fig. 2(b)]. The strength of the peaks is related to the thickness-to-width ratio of the patterned thin film, just as for the peak at the edge of a strip. This phenomenon has been analytically studied in the torus case,[24] where a similar negative peak on the inner edge of the torus is found.

To show this phenomenon in more detail, profiles along the line AB (Fig. 1) are shown for sample 2 at various applied fields in Fig. 3(a).

FIG. 2. (a) Schematic diagram showing magnetic field lines due to a current flowing in a ring of inner radius a_1, outer radius a_2, and thickness d, in the presence of an externally applied field. Near the outer edges of the ring, the local field is high, due to enhancement of the external field by the field generated by the current. At the inner edge of the ring, the external field is reduced by the field of the current. (b) Field profiles are shown schematically (dotted line) and indicate the sharp peak at the edges of the ring due to the large aspect ratio. The expected conventional magneto-optical intensity ($\sim H_{ext}^2$) is indicated by the black line.
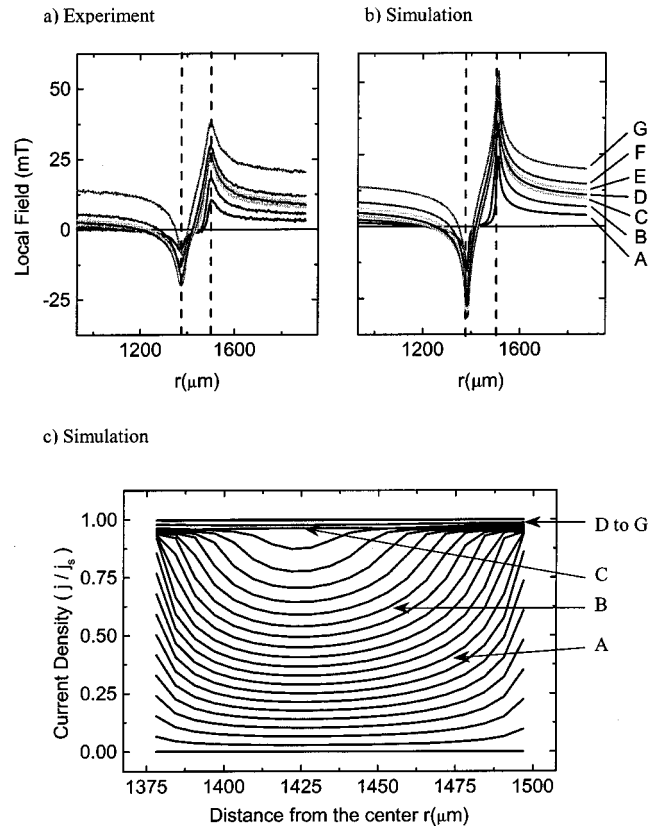
Also from the profiles it is clear that, as soon as an external field is applied, some negative field is present at the inner edge of the ring. The spatial distribution of the field inside the hole of the ring is dome shaped, which is particularly clear at higher applied fields.

The negative peak at the inner edge of the ring initially becomes stronger with increasing external field. This is due to an increase in total current flowing in the ring, because the width of the region where j_s flows increases with external field. At a certain external field, i.e., the penetration field, the maximum current density j_s flows everywhere in the ring (approximately, see below). The total current in the ring cannot increase anymore and therefore the self-field due to the shielding currents is constant. The only effect of an increasing external field is now a shifting of the whole field profile upwards. This implies that the negative field at the inner edge henceforth decreases in strength until it becomes positive.

In Fig. 4 we show magneto-optical images for sample 1 obtained with conventional magneto-optical imaging where the intensity is proportional to the square of the local field. In such images, both the outer and inner peaks appear bright. The inner peak first increases in brightness with applied field, then decreases, fully consistent with the initial increase and subsequent decrease in magnitude of the field as explained above.

To investigate the behavior described above in more detail, we present the results of our simulation, as outlined in Sec. III. The simulation yields both the current density distribution and the corresponding field distribution during a hysteresis loop.

FIG. 3. (a) Experimental MO-ILIA (see text) field profiles and (b) calculated field profiles (from bottom to top) for $\mu_0 H_{ext}$ $=3$ mT (A), 5.5 mT (B), 7.9 mT (C), 9.1 mT (D), 10.5 mT (E), 12.7 mT (F), and 18 mT (G), in ring 2 as a function of the distance r from the center of the ring. The positions of these fields in the hysteresis loop are indicated in Fig. 5. The dotted lines indicate the inner and outer edge of the ring. (c) Local current density from ZFC (bottom) to full penetration (top) as a function of position in the ring, given in units of j_s. The characters $A-G$ indicate the external field and are defined above. *A color version of Fig. 3 is available at* http://www.nat.vu.nl/CondMat/colfigs/2001/mp-prbr.htm

The results for first penetration from the ZFC situation, where initially the current density j is zero all over the width of the ring, up to the state of full penetration, where $j \simeq j_s$, are shown in Figs. 3(b) and 3(c). The corresponding points on the calculated and measured magnetization curves shown in Fig. 5 are indicated with the characters $A-G$.

Note that even at relatively high fields j only approaches but never reaches the true critical current density j_c for several reasons. First, due to relaxation (which is implicitly present also in the model due to the finite resistivity), one can never reach j_c, but obtains a lower value $j_s \lesssim j_c$. Second, we find from our simulations that j_s depends on the radial position, it maximum value is reached at the outer perimeter due to the geometry (although the difference is rather small). For the normalization in Figs. 3(c) and 6(c) we took the outer edge value. Third, see [see Fig. 3(c)], at one-third from the inner edge of the ring there is a dip in j, which disappears only very slowly with increasing field. The effect on magnetization is, however, rather small; for instance, the magnetization for curve B is only 15% lower than the maxi-
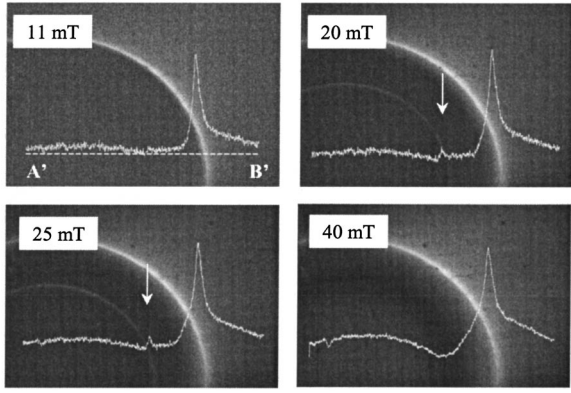
FIG. 4. Experimental conventional magneto-optical intensity images (proportional to the local field squared), for $\mu_0 H_{ext} = 11$, 20, 25, and 40 mT, on ring 1, at $T = 4.2$ K. The profiles along the dashed line $A'B'$ are shown in the picture. We note that a small peak starts to appear at the inner edge of the ring at 20 mT (see arrow) and reaches a maximum at 25 mT, then decreases and disappears at 40 mT, while the high-intensity peak at the outer edge of the ring keeps on increasing (for a discussion, see text). This implies for the penetration field that $\mu_0 H_p = 25$ mT.

mum magnetization. From this it is immediately clear that there is not a sharply defined penetration field. Rather there is an abrupt but continuous change between increasing magnetization and constant magnetization.

We note that the maximum of the inner peak in Fig. 3(a), curve C, occurs for the situation where, for the first time after zero field cooling, $j \cong j_s$ over the whole superconducting sample [Fig. 3(c), curve C]. Therefore the maximum in the inner peak as a function of applied field can be used as an accurate magneto-optical determination of the value of the penetration field H_p. To confirm this, we compare the values for H_p obtained according to this criterion with the values for H_p measured from torque.

The results for the two rings are as in Table I.

Clearly, the two results for H_p are in good agreement, which means that the global method used in torque to mea-
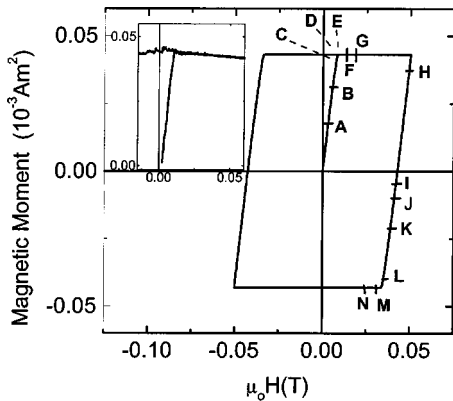

FIG. 5. Calculated hysteresis loop starting from ZFC conditions. The characters refer to the curves in Fig. 3 (A–G) and Fig. 6 (H–N). Inset: part of the experimental magnetization loop from torque measurements. The letters refer to the curves in Fig. 3(a) (A–G).
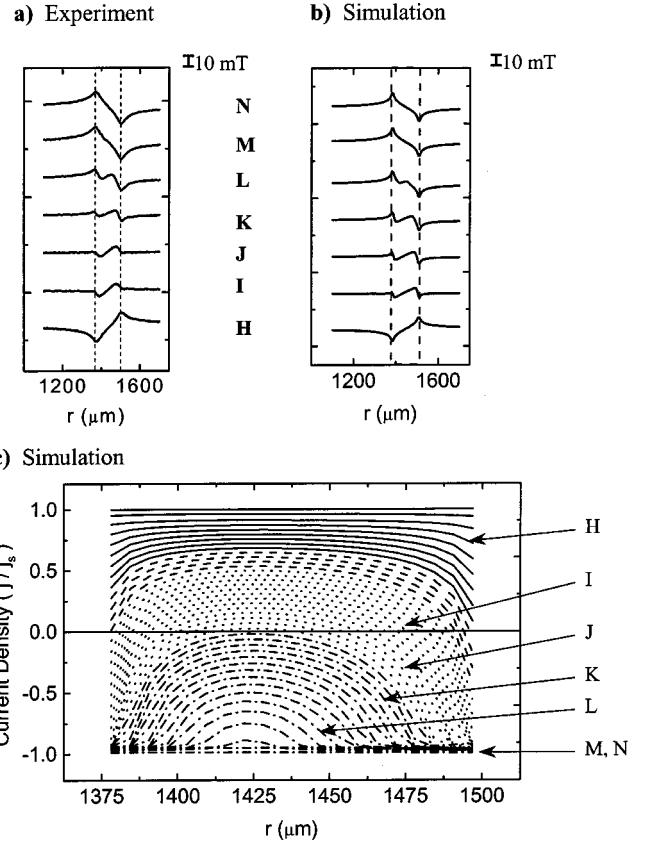

FIG. 6. (a) Experimental MO- ILIA profiles and (b) calculated profiles in the narrow ring during field reversal, for (from bottom to top) $\mu_0 H_{ext} = 49$ mT (H), 42 mT (I), 41 mT (J), 39 mT (K), 35 mT (L), 31 mT (M), and 24 mT (N). The positions of these fields on the hysteresis loop are indicated in Fig. 5. The dotted lines indicate the inner and outer edges of the ring. Note that the scale 10 mT gives the scale within one profile curve. The curves are shifted vertically for clarity. (c) Local current density during field reversal, from the full penetration of a positive applied field ($j = j_s$, top curve) to the full penetration due to a negative applied field ($j = -j_s$, bottom curve). The solid lines correspond to the regime where the currents are all positive within the ring. The dashed lines correspond to currents being mainly positive but negative on the outer edge. The dotted lines correspond to presence of negative-positive-negative currents. And the dot-dashed lines describe the regime where the currents are negative everywhere in the ring.

sure the penetration field is validated by the magneto-optical observation of the flux penetration under the same conditions. On the other hand, it is obvious, from Fig. 3, that before this full penetration state is reached, the current flowing in the ring is far from uniform. In the beginning there are even two regions with current flowing, separated by a Meiss-

TABLE I. Comparison of the penetration field H_p as obtained from torque and magneto-optical measurements.

	$\mu_0 H_p^{Torque}$ (mT)	$\mu_0 H_p^{MO}$ (mT)
Ring 1	25.5 ± 0.5	25 ± 1
Ring 2	10.0 ± 0.5	10.0 ± 1

TABLE II. Comparison of current density j_s as obtained from torque and magneto-optical measurements.

	$j_s^{Torque}(T=4.2\ \text{K})$	$j_s^{MO}(T=4.2\ \text{K})$
Ring 1	$3.9\times10^{11}A/m^2$	$4.19\times10^{11}A/m^2$
Ring 2	$5.3\times10^{11}A/m^2$	$6.82\times10^{11}A/m^2$

ner area. We will see an even more complicated current distribution pattern below, in the region where the field profile is reversed, immediately after reversing the sweep direction.

From the magneto-optically observed penetration fields H_p we also calculate the current density j_s using the formulas from Brandt:[10]

$$\frac{H_p}{j_s d} = \frac{2}{\pi}\left(\frac{1-x}{1+x}\right)\left[\ln 4\left(\frac{1+x}{1-x}\right) - 0.307\right] \quad \text{for} \quad x \geq 0.8, \tag{13}$$

$$\frac{H_p}{j_s d} = \frac{2p}{\pi}\left(\ln\frac{8}{p} - 1\right) - \frac{1}{2}(\ln x + 1 - x) \quad \text{for} \quad 0.6 < x < 0.8, \tag{14}$$

$$\frac{H_p}{j_s d} = \frac{1}{2}(-\ln x + 0.467) \quad \text{for} \quad x \leq 0.6, \tag{15}$$

where a_1 is the inner radius of the ring, a_2 the outer radius, $x = a_1/a_2$, and $p = (1-x)/(1+x)$. The first and last formulas are exact, while the middle is an interpolation. In our case $x = a_1/a_2 = 0.67$ for ring 1 and $x = 0.92$ for ring 2.

The values for j_s obtained in this manner magneto-optically and from the irreversible magnetization in the torque experiment from Eq. (4) are given in Table II. The magneto-optical values for j_s are slightly higher than from the torque measurements, but the agreement is very reasonable.

B. Field reversal

We observe a rather surprising behavior of the flux during field reversal. The profiles measured on sample 2 are shown in Fig. 6(a), while the corresponding points in the hysteresis curve are again indicated in Fig. 5. The profile shown at the bottom (curve H) is the well-known curve for full penetration in a positive applied field. From bottom to top the applied field $\mu_0 H_{ext}$ is decreased from 49 to 24 mT, the latter field being after the complete reversal of the profile. A further decrease of $\mu_0 H_{ext}$, first to zero applied field and then to negative applied field, only leads to a vertical shift of the curve, but no change in shape is observed. Note that between 49 and 24 mT, the profile goes through a quite complex

sequence of patterns, e.g., at $\mu_0 H_{ext} = 35$ mT (curve L), four peaks (counting both positive and negative peaks) are present in the ring. From the slope dB_z/dr, where r is the radial distance from the center of the ring, one gets the impression that there are two counterrotating current loops in the ring. To investigate this further, we compare now the experiment with simulations.

Results for the current and field profiles from the numerical simulation as described in Sec. III, are shown in Figs. 6(b) and 6(c). Note the nice correspondence between the experimental and the simulated field profiles shown in Figs. 6(a) and 6(b). From the simulated curves in Fig. 6(c) it is clear that during field reversal, the current changes smoothly from, say, a clockwise direction (positive j) to an anticlockwise direction (negative j). This happens, however, in a nonuniform manner over the width of the ring. First the current becomes negative at the outside edge of the ring, while at the inside there is still a positive current flowing. Hence during this crossover, there are two antiparallel currents flowing along the whole circumference of the ring. After further reduction of the external field also a negative current starts to flow at the inner edge. In the middle of the ring, however, there is still a positive current flowing. That is, we have three concentric currents loops, with antiparallel flow in adjacent ones. When the external field is further reduced, also in the middle of the ring negative currents start to flow and the flow *direction* becomes uniform again. Upon reaching $H_{max} - 2H_p$, the current density becomes nearly uniform again.

V. CONCLUSIONS

We have experimentally studied the flux penetration in a superconducting ring, by torque magnetometry and local magneto-optical observations, which allow direct determination of the magnetic field. At the first flux penetration after ZFC, immediately some flux is present inside the hole of the ring, peaking at the inner edge. This is due to closure of the field lines generated by the shielding current. We have shown by simulations that the maximum value of the inner peak occurs at the penetration field H_p, in good agreement with H_p determined by torque measurements. Another interesting feature is the complicated field and current pattern just after reversal of the field sweep direction. Despite the small width of the rings, three concentric current loops are found.

*After November 2001 at CEA Saclay, SPEC, DRECAM, F-91191 Gif Sur Yvette, France.

†Corresponding author. Electronic address: rw@nat.vu.nl

[1] E.V. Matizen, P.P. Bezverkhy, V.G. Martynets, and S.M. Ishikaev, Phys. Rev. B **59**, 9649 (1999).

[2] S.A.L. Foulds, J. Smithyman, G.F. Cox, C.M. Muirhead, and R.G. Humphreys, Phys. Rev. B **55**, 9098 (1997).

[3] H. Zheng, M. Jiang, R. Nikolova, V. Vlasko-Vlasov, U. Welp, B.W. Veal, G.W. Crabtree, and H. Claus, Physica C **309**, 17 (1998).

[4] I.L. Landau and H.R. Ott, Phys. Rev. B **61**, 727 (2000).

[5] F.C. Klaassen, G. Doornbos, J.M. Huijbregtse, R.C.F. van der

Geest, B. Dam, and R. Griessen (unpublished).

[6] B. Dam, J.M. Huijbregtse, F.C. Klaassen, R.C.F. van der Geest, G. Doornbos, J.H. Rector, A.M. Testa, S. Freisem, J.C. Martinez, B. Stäuble-Pümpin, and R. Griessen, Nature (London) **399**, 439 (1999).

[7] A.J.J. van Dalen, R. Griessen, S. Libbrecht, Y. Bruynseraede, and E. Osquiguil, Phys. Rev. B **54**, 1366 (1996).

[8] I.L. Landau and H.R. Ott, Physica C **331**, 1 (2000).

[9] Th. Herzog, H.A. Radovan, P. Ziemann, and E.H. Brandt, Phys. Rev. B **56**, 2871 (1997).

[10] E.H. Brandt, Phys. Rev. B **55**, 14 513 (1997).

[11] M.R. Koblischka and R.J. Wijngaarden, Supercond. Sci. Technol. **8**, 199 (1995).

[12] A.E. Pashitski, A. Gurevich, A.A. Polyanskii, D.C. Larbalestier, A. Goyal, E.D. Specht, D.M. Kroeger, J.A. DeLuca, and J.E. Tkaczyk, Science **275**, 367 (1997).

[13] R.J. Wijngaarden, H.J.W. Spoelder, R. Surdeanu, and R. Griessen, Phys. Rev. B **54**, 6742 (1996), and references therein.

[14] R.J. Wijngaarden, K. Heeck, H.J.W. Spoelder, R. Surdeanu, and R. Griessen, Physica C **295**, 177 (1998).

[15] R.J. Wijngaarden, K. Heeck, M. Welling, R. Limburg, M. Pannetier, K. van Zetten, V.L.G. Roorda, and A.R. Voorwinden, Rev. Sci. Instrum. **72**, 2661 (2001).

[16] J.M. Huijbregtse, B. Dam, J.H. Rector, and R. Griessen, J. Appl. Phys. **86**, 6528 (1999).

[17] Jeroen Huijbregtse, Ph.D. thesis, Vrije Universiteit Amsterdam, 2001.

[18] M. Qvarford, K. Heeck, J.G. Lensink, R.J. Wijngaarden, and R. Griessen, Rev. Sci. Instrum. **63**, 5726 (1992).

[19] L.A. Dorosinskii, M.V. Indenbom, V.I. Nikitenko, Yu. A. Ossip'yan, A.A. Polyanskii, and V.K. Vlasko-Vlasov, Physica C **216**, 205 (1993).

[20] R.J. Wijngaarden, R. Griessen, J. Fendrich, and W.K. Kwok, Phys. Rev. B **55**, 3268 (1997).

[21] J.D. Jackson, *Classical Electrodynamics,* 2nd ed. (Wiley, New York, 1975), p. 173.

[22] M. Baziljevich, Ph.D. thesis, University of Oslo, 1996.

[23] E.H. Brandt and M. Indenbom, Phys. Rev. B **48**, 12 893 (1993).

[24] V. Ivaska, V. Jonkus, and V. Palenskis, Physica C **319**, 79 (1999).